The Cerebellum (2018) 17:709–721
https://doi.org/10.1007/s12311-018-0966-x

ORIGINAL PAPER

Cellular and Subcellular Localization of Endogenous Neuroligin-1 in the Cerebellum

Kazuya Nozawa[1] · Ayumi Hayashi[1] · Junko Motohashi[1] · Yukari H. Takeo[1] · Keiko Matsuda[1] · Michisuke Yuzaki[1]

Published online: 25 July 2018

Abstract

Synapses are precisely established, maintained, and modified throughout life by molecules called synaptic organizers, which include neurexins and neuroligins (Nlgn). Despite the importance of synaptic organizers in defining functions of neuronal circuits, the cellular and subcellular localization of many synaptic organizers has remained largely elusive because of the paucity of specific antibodies for immunohistochemical studies. In the present study, rather than raising specific antibodies, we generated knock-in mice in which a hemagglutinin (HA) epitope was inserted in the *Nlgn1* gene. We have achieved high-throughput and precise gene editing by delivering the CRISPR/Cas9 system into zygotes. Using *HA-Nlgn1* mice, we found that HA-Nlgn1 was enriched at synapses between parallel fibers and molecular layer interneurons (MLIs) and the glomeruli, in which mossy fiber terminals synapse onto granule cell dendrites. HA immunoreactivity was colocalized with postsynaptic density 95 at these synapses, indicating that endogenous Nlgn1 is localized at excitatory postsynaptic sites. In contrast, HA-Nlgn1 signals were very weak in dendrites and somata of Purkinje cells. Interestingly, HA-immunoreactivities were also observed in the pinceau, a specialized structure formed by MLI axons and astrocytes. HA-immunoreactivities in the pinceau were significantly reduced by knockdown of Nlgn1 in MLIs, indicating that in addition to postsynaptic sites, Nlgn1 is also localized at MLI axons. Our results indicate that epitope-tagging by electroporation-based gene editing with CRISPR/Cas9 is a viable and powerful method for mapping endogenous synaptic organizers with subcellular resolution, without the need for specific antibodies for each protein.

Keywords Mouse · Cerebellum · Neuroligin · Pinceau · CRISPR/Cas9 · Synapse

Introduction

Changes in neuronal connectivity, which can be assessed by various imaging techniques in the living human brain, are thought to underlie certain neurodevelopmental and neuropsychiatric disorders [1, 2]. At the molecular level, synaptic connections are formed, maintained, or eliminated by molecules collectively referred to as synaptic organizers, which include various secreted factors and cell adhesion molecules, such as neurexins (Nrxns) and neuroligins (Nlgns) [3, 4]. Interestingly, the same synaptic organizers can regulate different aspects of synaptic properties, in a context-dependent manner. For example, a triple knockout of the *Nlgn1–Nlgn3* genes in cerebellar Purkinje cells (PCs) caused an ~80% reduction in inhibitory transmission at molecular layer interneuron (MLI)–PC synapses, without affecting excitatory transmission at parallel fiber (PF; axons of granule cells)–PC synapses [5]. In contrast, the triple knockout of *Nlgn1–Nlgn3* genes in MLIs did not affect inhibitory synapses between MLIs, but reduced excitatory synaptic transmission mediated by N-methyl-D-aspartate (NMDA)-type glutamate receptors at PF–MLI synapses [6]. Thus, it is likely that even in the same neurons, distinct sets of synaptic organizers are differentially transported to and localized at specific synapses. Therefore, the first step to understand how specific neuronal circuits are regulated is to precisely map various synaptic organizers with subcellular resolution at each synapse.

Despite decades of research, however, the number of antibodies that can be used for immunohistochemical detection of endogenous synaptic organizers is surprisingly limited. For example, all seven antibodies used for detecting Nlgn1 in earlier studies show non-specific immunoreactivities in *Nlgn1* knockout brain tissues [5]. The paucity of specific antibodies for immunohistochemical studies is partly because

✉ Michisuke Yuzaki
myuzaki@keio.jp

[1] Department of Physiology, Keio University School of Medicine, Tokyo 160-8582, Japan

synapses contain abundant proteins that share intricate molecular interactions with each other, which might mask certain epitopes of synaptic organizers [7]. In addition, a high degree of amino acid sequence similarity among various isoforms of synaptic organizers makes it difficult to develop specific antibodies. An alternative approach to localize synaptic organizers is to overexpress proteins fused with epitope tags or fluorescent proteins. A caveat of this approach is that overexpression can cause mistargeting of the expressed protein and potential changes in synaptic functions. A better option is to insert a sequence encoding an epitope tag or fluorescent protein into a gene of interest using gene knock-in technologies [8]. However, generation of knock-in mice using conventional homologous recombination methods in embryonic stem cells is labor-intensive and time-consuming, prohibiting high-throughput mapping of endogenous synaptic proteins.

Recent advances in genome editing using the clustered regularly interspaced short palindromic repeats (CRISPR)-associated endonuclease Cas9 have enabled efficient insertion of an epitope into precise genomic locations by co-injection of Cas9 mRNA, guide RNAs (gRNAs), and donor DNAs into zygotes [9]. However, microinjection is a special skill and it is time-consuming to produce mutant mice on a large scale. By delivering the CRISPR/Cas9 editing machinery through in utero electroporation, in vivo genome editing was also able to insert a sequence encoding an epitope tag to a gene of interest [10]. Although the latter technique provides a high-throughput platform for determining the subcellular localization of endogenous proteins in single neurons, mapping of synaptic organizers at the level of neuronal circuits and in various brain regions requires global genome editing in zygotes. In the present study, we employed a high-throughput electroporation method to introduce the editing machinery into zygotes [11, 12]. As a proof-of-principle of this approach, we generated a knock-in mouse line in which a hemagglutinin (HA) epitope was inserted in the *Nlgn1* gene by electroporation-based gene editing with CRISPR/Cas9 and performed cellular and subcellular immunohistochemical analyses of endogenous Nlgn1 proteins in cerebellar circuits. We found that Nlgn1 was highly expressed at PF–MLI synapses in the molecular layer and the cerebellar glomerulus in the granular layer, with very low expression in Purkinje cells. Furthermore, we found that Nlgn1 expression in MLI axons occurs at the cerebellar pinceau formation.

Materials and Methods

Animals

All procedures related to animal care and treatment were performed in accordance with the guidelines approved by the animal resource committees of Keio University. Mice were housed in a 12:12 h light-dark cycle with food and water available ad libitum. A combination anesthetic (0.3 mg/kg of medetomidine, 4.0 mg/kg of midazolam, and 5.0 mg/kg of butorphanol) [13] was administered by intraperitoneal injection before surgery or transcardial perfusion. We used B6D2F1 (C57BL/6 x DBA2 F1) mice (SLC, Shizuoka, Japan) at 2–6 months of age. ICR mice (SLC) were used as controls.

Generation of HA-Tagged *Nlgn1* Knock-in Mice

B6D2F1 female mice (4 weeks old) were super-ovulated by intraperitoneal injection of pregnant mare's serum gonadotropin (PMSG, 5 IU; ASKA Animal Health, Tokyo, Japan). Forty-eight hours later, mice were injected with human chorionic gonadotropin (hCG, 5 IU; ASKA Animal Health) and mated with B6D2F1 males. Zygotes were collected from the oviducts of female mice at embryonic day (E) 0.5. The covering cumulus cells were removed by incubation in 1% hyaluronidase/M2 medium (Millipore Sigma, MA, USA). SpCas9 protein (250 ng/μl; PNA Bio, Newbury Park, CA, USA), *Nlgn1*-crRNA (5 pmol/μl, 5'-UC ACG UAC UCU CUC AAA AGU GUU UUA GAG CUA UGC UGU UUU g-3′), trans-activating crRNA (5 pmol/μl; Fasmac, Kanagawa, Japan), and 200-bp single-stranded oligodeoxynucleotide (ssODN, 500 ng/μl; 5′-GAG CTA TGA TGG CAT GTG TGG TCC ACA GGG GAT CCG GTG CCC CAT TGA CTC TCT GCT TGT TGG GAT GTT TGC TAC AGA CTT TTC ACG TAC TCT CTC AAA AGT ACC CAT ACG ACG TGC CAG ACT ACG CTT TGG ATG ATG TAG ACC CAT TGG TTA CTA CTA ACT TTG GCA AGA TTA GGG GAA TTA AGA AAG AA-3′; Integrated DNA Technologies, IA, USA), which harbored a sequence encoding an HA tag flanked by homologous arms corresponding to exon 3 of *Nlgn1*, were incubated at 37 °C for 15 min before electroporation. Electroporation was performed using platinum block electrodes (150 mA, [1 msec On +100 msec Off] for 2 pulses; GE-101, BEX, Tokyo, Japan) connected to CUY21EDIT II (BEX). Zygotes were incubated at 37 °C in 5% CO_2 till they reached the two-cell stage and transferred into oviducts of pseudopregnant ICR females.

To investigate CRISPR/Cas9-mediated mutation in the *Nlgn1* gene, genomic DNA was prepared from mouse tails. The genomic regions flanking the gRNA target were amplified by PCR using specific primers: 5′- ACC ACC ATT CCA TCT TTC TCC -3′ and 5'-ACG TAT GAT GAA ACC ACA TCC -3′. The PCR amplicons were cloned into the pMD20 vector (Takara Bio, Shiga, Japan). The genomic region was sequenced from plasmids isolated from each mouse or directly from PCR amplicons. The results of sequencing were analyzed by CRISP-ID (http://crispid.gbiomed.kuleuven.be/) [14].

DNA Constructs

The cDNA encoding an HA tag (YPYDVPDYA) was added immediately after the signal sequence of mouse Nlgn1 cDNA, which lacked the insertion of the splice sites A and B (a gift from Dr. P. Scheiffele, University of Basel, Basel, Switzerland), and cloned into the pCAGGS vector (provided by Dr. J. Miyazaki, Osaka University, Osaka, Japan). The extracellular acetylcholinesterase (AChE) domain (amino acids 48–630 of mouse Nlgn1) was deleted to generate ΔAChE-Nlgn1. Nlgn1-Fc or HA-Nlgn1-Fc was generated by adding the immunoglobulin Fc fragment of human IgG1 to the 3′ end of the extracellular domain of Nlgn1 (amino acids 1-696). All mutations, which were introduced by two-step PCR amplification, were confirmed by sequencing.

Surface Biotinylation Assays in HEK293 Cells

Nlgn1 constructs were transfected into HEK293 cells by the calcium phosphate method. One day after transfection, the cells were incubated with 0.5 mg/ml Sulfo-NHS-LC-Biotin (Thermo Fisher Scientific, MA, USA) in isotonic bicarbonate buffer for 10 min and incubated with 1 M Tris (pH 7.5) to quench the biotinylating reaction. Cells were collected in TNE-SDS buffer (50 mM Tris, 10% NP40, 20 mM EDTA, 0.1% SDS) containing a protease inhibitor cocktail (set V; Millipore Sigma) and incubated for 30 min at 4 °C. Debris was removed by centrifugation, and the supernatants were incubated with NeutrAvidin agarose beads (Thermo Fisher Scientific) for 1 h at 4 °C. The beads were washed five times with lysis buffer and the bound proteins were eluted with sample buffer.

Cell-Based Binding Assay

Fc-Nlgn1 proteins were collected from the culture media of HEK293 cells 3 days after transfection. The protein concentration in the media was quantified by immunoblot analyses with anti-Fc antibody. HEK293 cells transfected with pCAGGS-Nrxn1β [15] were incubated with Fc-Nlgn1 proteins for 4 h in 96-well plates. The cells were fixed with phosphate buffered saline (PBS) containing 4% paraformaldehyde (PFA) for 10 min. After pre-incubation with blocking buffer (2% bovine serum albumin (BSA), 2% normal goat serum, detergent-free), cells were treated with rabbit anti-Fc primary antibody for 2 h, followed by HRP-conjugated anti-rabbit secondary antibody for 1 h. Chemiluminescence signals were obtained using a peroxidase substrate (SeraCare Life Science, MA, USA) for 10 min, and detected using a plate reader (Tecan, Männedorf, Switzerland).

Artificial Synapse Formation Assay

Hippocampal cultures were prepared from E17 mice as previously described [16]. An artificial synapse formation assay was performed by co-culturing with HEK293 cells expressing Nlgn1 or an empty vector, from 7 to 10 days in vitro (DIV), in the presence of 10 μM 5-fluoro-2-deoxyuridine, as described previously [17].

Immunoprecipitation

The cerebellum was dissected from anesthetized adult mice and homogenized in lysis buffer (20 mM Tris-HCl, 150 mM NaCl, pH 8.0) containing the protease inhibitor cocktail (cOmplete ULTRA, Roche, Basel, Switzerland). The homogenates were lysed with 1% Triton, and the soluble fraction was collected by centrifugation at 100,000×*g*. Protein concentration was calculated with a BCA assay kit (Pierce, Thermo Fisher) and standardized. Five hundred microliters of the soluble fraction was pre-cleared by Protein G sepharose (GE Healthcare, IL, USA) for 1 h, followed by overnight incubation with 1 μg primary antibody. Proteins were incubated with protein G-sepharose for 1 h, and bound proteins were separated and eluted by sample buffer containing 2-mercaptoethanol. Samples were analyzed by immunoblotting.

Immunohistochemistry

Mice were transcardially perfused with 4% PFA in 0.1 M phosphate buffer. Sagittal sections (50 μm thickness) of cerebellar vermis were prepared using a microslicer (DTK-1000, Dosaka EM, Kyoto, Japan). For staining of synaptic proteins, sections were treated with 1 mg/ml pepsin in 0.2 N HCl/PBS for 5 min at 37 °C. Sections were incubated with 10% normal donkey serum, followed by primary antibodies overnight, and then Alexa 405-, 488-, 647- (Molecular probe, Thermo Fisher), and Alexa 555 (Abcam, Cambridge, UK)-labeled species-specific secondary antibodies or 4′,6-diamidino-2-phenylindole (DAPI) for 1 h. Fluorescence images of confocal and super-resolution structured illumination microscopy (SIM) were captured using an SD-OSR microscope system (Olympus, Tokyo, Japan) equipped with a CSU-W1 scan unit (Yokogawa Electronics, Tokyo, Japan) and an ORCA-Flash 4.0 CMOS camera (Hamamatsu Photonics, Shizuoka, Japan). For measurement of HA puncta, Fiji software [18] was used to select puncta and to measure the intensity and size of the puncta.

For immunostaining of the synapse formation assay, cells were fixed in 4% PFA for 10 min, followed by 100% methanol at −20 °C. The cells were treated with blocking buffer (2% BSA, 2% normal goat serum, 0.1%

Triton-X100), followed by the primary antibody for 2 h and Alexa-conjugated secondary antibody for 1 h. Immunofluorescence images were captured using a CCD camera (DP80, Olympus) attached to a fluorescence microscope (BX51, Olympus). For measurement of vGluT1 intensity, fluorescent intensity was averaged in Nlgn1 or GFP-positive cell areas.

Primary Antibody

The following primary antibodies were obtained commercially: anti-vGluT1 (Goat, Frontier Science, Hokkaido, Japan), anti-Nlgn1 (mouse, NeuroMab, CA, USA), anti-Human IgG (Fc-specific, rabbit, Millipore Sigma), anti-HA.11 (mouse monoclonal, BioLegend, CA, USA), anti-HA (Rat, Roche), anti-HA (Rabbit monoclonal, Cell Signaling Technology, MA, USA), anti-Car8 (rabbit, Frontier Science), anti-parvalbumin (goat, Frontier Science), anti-PSD95 (guinea pig, Frontier Science), anti-MAP2 (mouse, Millipore), anti-3-phosphoglycerate dehydrogenase (3-PGDH; guinea pig, Frontier Science), anti-GFP (guinea pig, Frontier Science), and anti-GFP (rabbit, Frontier Science).

Gene Knockdown Using Adeno-Associated Virus

To knockdown Nlgn1, we constructed shRNA using the specific target sequence of Nlgn1 that has been described previously [19]: GGA AGG UAC UGG AAA UCU G. The shRNA was inserted under the H1 promoter of the pAAV-CAG-GFP vector (#37825; Addgene, MA, USA). As a negative control, no shRNA was inserted. To test knockdown efficiency of shRNA constructs, HEK293 cells were co-transfected with AAV-DJ vector and pCAGGS-HA-Nlgn1. Cells were lysed with TNE-SDS buffer 3 days after transfection, and the HA-Nlgn1 levels were analyzed by immunoblotting.

To produce virus particles, the shRNA construct, pAAV-DJ (Cell Biolabs, Inc., CA, USA), and pHelper (AAV Helper-Free system, Agilent Technologies, CA, USA) were co-transfected into AAV293 cells (Agilent Technologies) with lipofectamine 2000 (Invitrogen, Thermo Fisher) and incubated for 3 days in the presence of 1 μM tricostatin A. After three freeze-thaw cycles, cells were centrifuged at 600×*g* for 30 min to remove debris. Virus particles were purified from the supernatant with the AAV purification kit (VIRAPUR, CA, USA) and concentrated by filter units (Millipore Sigma) according to manufactures' protocols. Two microliters of the virus solution were injected into the cerebellum as described previously [20], and mice were sacrificed at 14 to 21 days after the injection (dpi 14–21) for immunohistological analyses.

Results

Addition of HA Tag Does Not Affect Nlgn1 Location and Function In Vitro

HA-Nlgn1, in which an HA epitope was added at the N-terminus of Nlgn1 after the signal sequence, was previously shown to be transported to postsynaptic sites and induce synapses when overexpressed [19, 21]. However, whether addition of an HA tag affects trafficking and function of Nlgn1 was unclear. To address this question, we first examined trafficking of HA-Nlgn1 by cell-surface biotinylation assays in HEK293 cells. Immunoblot analyses using anti-Nlgn1 antibody revealed that Nlgn1 and HA-Nlgn1 were similarly localized on the cell surface (Fig. 1a).

Next, we examined whether addition of the HA tag affected binding of Nlgn1 to its receptor Nrxn, using cell-based binding assays. The extracellular domain of Nlgn1 or HA-Nlgn1 was fused to the Fc fragment of IgG to prepare soluble Nlgn proteins and then added to HEK293 cells expressing Nrxn1β. Chemiluminescent-based quantification of cell surface Fc-proteins revealed that Nlgn1-Fc and HA-Nlgn1-Fc bind to Nrxn1β on HEK293 cells in a similar manner (Fig. 1b).

Finally, we tested the effect of the HA tag on synaptogenic activities of Nlgn1 by performing an artificial synapse formation assay [22]. Hippocampal neurons were co-cultured with HEK293 cells expressing green fluorescent protein (GFP), plus Nlgn1 or HA-Nlgn1. Immunocytochemical analyses of presynaptic terminals using an antibody against vesicular glutamate transporter (vGluT1), a presynaptic marker for glutamatergic synaptic vesicles, revealed that Nlgn1 and HA-Nlgn1, but not GFP alone or Nlgn1 lacking the extracellular AChE domain (Nlgn1-ΔAChE), induced the formation of presynaptic structures on HEK293 cells (Fig. 1c); the effect induced by Nlgn1 and HA-Nlgn1 was similar. Together, these results indicate that addition of the HA tag to the N-terminus does not affect cell surface trafficking, binding, or synaptogenic activity of Nlgn1, at least in vitro.

Generation of *HA-Nlgn1* Knock-in Mice by Electroporation

To achieve efficient genome editing in mouse zygotes, we first optimized the electroporation conditions by monitoring the fluorescence intensity of GFP, which was introduced as mRNA, and the rate of embryo survival to the blastocyst stage [11]. Although acidic Tyrode's solution treatment was used earlier [12], we found that a short current pulse (150 mA for 1 msec) repeated twice in 100 msec was sufficient to introduce mRNA into mouse zygotes without the Tyrode's treatment (Fig. 2a). Using these conditions, we introduced pre-assembled SpCas9/gRNA complex and a donor ssODN into 66 zygotes in a single electroporation (Fig. 2b). Sixty-three

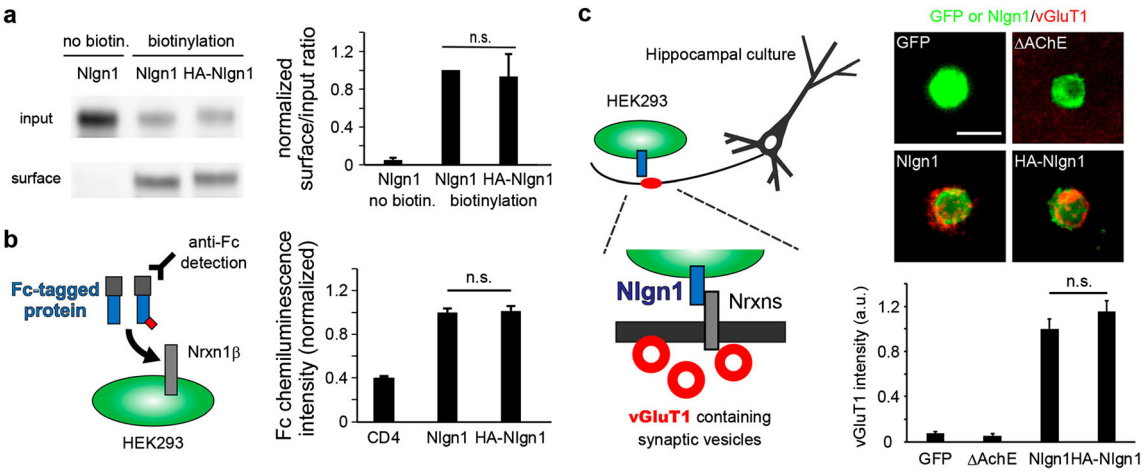

Fig. 1 Addition of an HA tag does not affect Nlgn1 location and function in vitro. **a** Cell-surface biotinylation assays. HEK293 cells expressing Nlgn1 or HA-Nlgn1 were cell-surface biotinylated. Total cell lysates (input) and the biotinylated fraction (surface) were subjected to immunoblot assays using anti-Nlgn1 antibody (left). The right graph indicates the quantified ratio of surface to total immunopositive bands from HEK293 cells expressing Nlgn1 (with and without biotinylation) and HA-Nlgn1. n.s, not significant based on the Kruskal-Wallis test and Steel-Dwass post hoc test. $n = 3$ independent experiments. **b** Cell-based binding assays. The extracellular domain of Nlgn1 or HA-Nlgn1 was fused to the Fc fragment to prepare soluble Nlgn1 proteins and then added to HEK293 cells expressing Nrxn1β (left). The right graph indicates chemiluminescent-based quantification of cell surface Fc-proteins in HEK293 cells expressing CD4, Nlgn1, or HA-Nlgn1. n.s., not significant based on the Kruskal-Wallis test and Steel-Dwass post hoc test. $n = 3$ independent experiments. **c** Artificial synapse formation assays. Hippocampal neurons were co-cultured with HEK293 cells expressing GFP plus Nlgn1 or HA-Nlgn1. Artificial synapses formed on HEK293 cells were visualized by immunostaining of vGluT1 (left). Representative images of artificial synapses (vGluT1, red) formed on HEK293 cells (GFP, green) are shown on the right. Scale bar, 5 μm. The bottom graph shows quantification of vGluT1 intensity in GFP-positive areas, in HEK293 cells expressing GFP alone, Nlgn1-ΔAChE, Nlgn1, or HA-Nlgn1. n.s., not significant based on the Kruskal-Wallis test and Steel-Dwass post hoc test. $n > 100$ cells from three independent experiments. Data in all graphs represent means ±SEM

zygotes that survived to the two-cell stage were transferred into pseudopregnant females. Genomic DNA sequencing revealed that six mice, out of 18 F0 mice, contained the HA-encoding sequence at the targeted site of the *Nlgn1* gene (Fig. 2c). Germline transmission of the *HA-Nlgn1* gene was also confirmed by genomic sequencing of the F1 offspring.

To confirm the expression of the HA-Nlgn1 protein, we first performed immunoblot assays using anti-Nlgn1 antibody. We detected Nlgn1-immunopositive ~100 kDa bands after immunoprecipitation of brain lysates with anti-HA antibody only from *HA-Nlgn1* mice, but not wild-type mice (Fig. 2d). Similarly, anti-Nlgn1 antibody immunoprecipitated HA-immunopositive ~100 kDa bands only in *HA-Nlgn1*, but not in wild-type mice (Fig. 2e, middle two lanes), indicating that HA-Nlgn1 proteins are specifically expressed in *HA-Nlgn1* mice.

A concern with using CRISPR/Cas9-based gene editing is that the epitope tag may be inserted in coding sequences of unrelated genes. We assessed this possibility by immunoblotting with anti-HA antibody after immunoprecipitation of HA-tagged proteins to enrich and detect HA-tagged proteins in brain lysates. We only detected ~100 kDa bands corresponding to Nlgn1 and non-specific bands corresponding to antibodies in *HA-Nlgn1* knock-in mice (Fig. 2e). Taken together, we obtained *HA-Nlgn1* knock-in mice efficiently by CRISPR/Cas9-based gene editing using electroporation into zygotes.

Nlgn1 Is Enriched in MLIs and GCs but Not in PCs in the Cerebellum

To analyze cellular localization of endogenous Nlgn1 in the cerebellum, we performed immunohistochemical analyses using antibodies against HA, carbonic anhydrase 8 (Car8, a marker for PCs), and parvalbumin (PV, a marker for PCs and MLIs), together with nuclear staining with DAPI. HA immunoreactivity was observed throughout the cerebellum of *HA-Nlgn1* mice, but not in wild-type mice (Fig. 3a), indicating the specificity of the anti-HA antibody for immunohistochemical studies. In the molecular layer, HA immunoreactivity was highly enriched in Car8-negative but PV-positive dendrites and somata in the superficial layer (Fig. 3a, box 1) and the deep layer, near PCs (Fig. 3a, box 2), indicating Nlgn1 expression in both stellate- and basket-cell types of MLIs. In contrast, HA-Nlgn1 immunoreactivity was very weak in Car8- and PV-positive PCs (Fig. 3a, box 3). Indeed, ~80% of HA-immunopositive puncta were negative for Car8 in the molecular layer (Fig. 3b), indicating that Nlgn1 was mostly located in the MLIs. Nlgn1 was also observed in cerebellar glomeruli (Fig. 3a, box 4), in which mossy fiber terminals synapse onto granule cell dendrites. These results indicate that cell-specific localization of endogenous Nlgn1 can be mapped in the cerebellum of *HA-Nlgn1* mice.

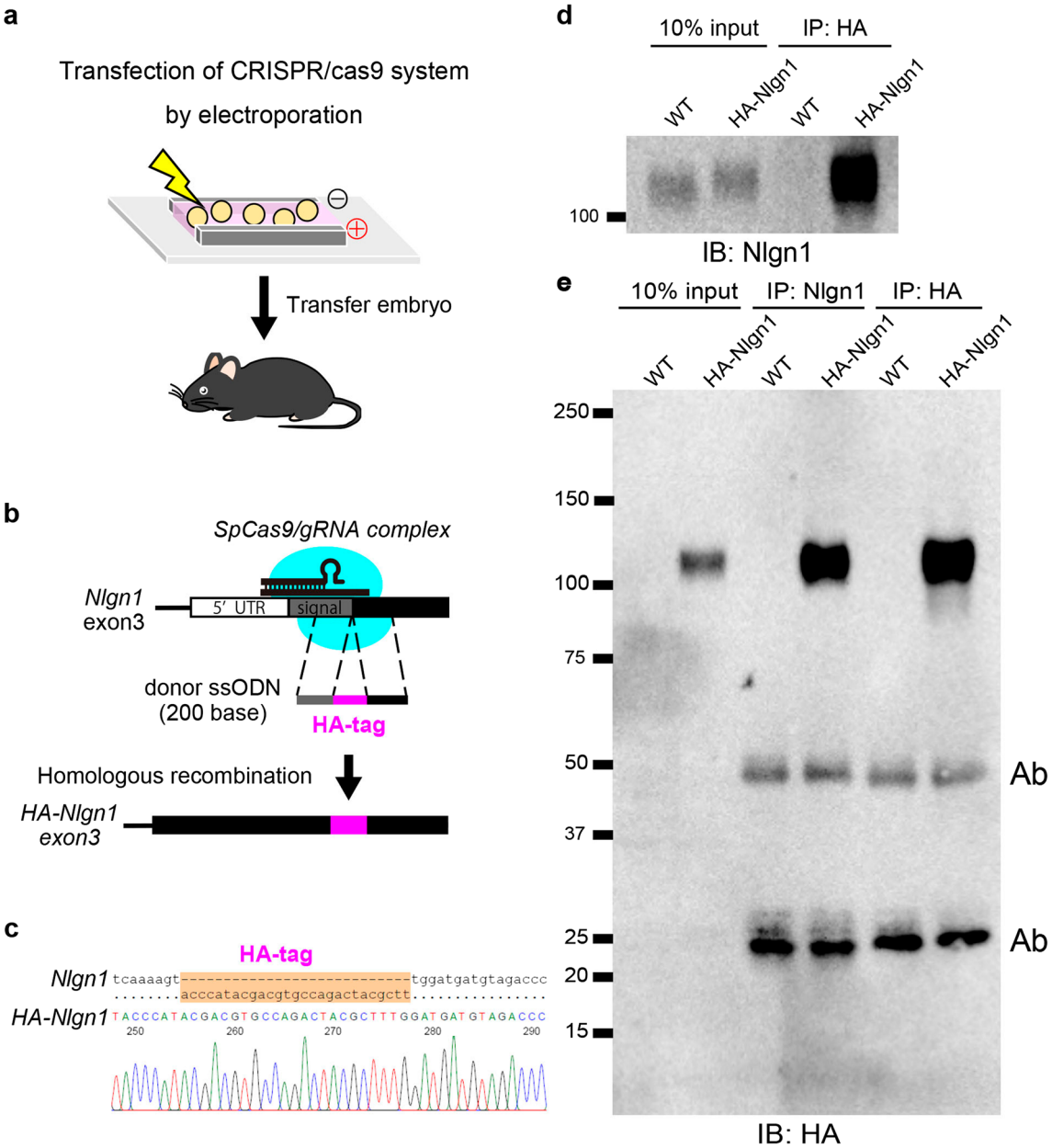

Fig. 2 Generation of *HA-Nlgn1* knock-in mice by electroporation-based gene editing with CRISPR/Cas9. **a** Schematics of electroporation-based introduction of the CRISPR/Cas9 editing machinery into zygotes. **b** Schematics of the knock-in strategy. A donor ssODN (200 bp) and the gRNA were designed to knock-in a sequence encoding an HA tag immediately after the signal sequence located at exon 3 of the *Nlgn1* gene. **c** Representative genomic DNA sequencing data indicating the correct knock-in of the HA tag. **d** Expression of the HA-Nlgn1 protein in *HA-Nlgn1* mice. A representative immunoblot shows Nlgn1-immunopositive bands in cerebellar lysates solubilized by Triton-X (10% input, left two lanes) from both wild-type (WT) and *HA-Nlgn1* mice. The Nlgn1-immunopositive band was also detected after immunoprecipitation of the lysates using anti-HA antibody (IP, right two lanes), only in *HA-Nlgn1* mice. **e** A representative immunoblot shows HA-immunopositive bands at ~100 kDa in cerebellar lysates (lane 2), and those after immunoprecipitation with anti-Nlgn1 (lane 4) or anti-HA (lane 6) antibodies, in *HA-Nlgn1*, but not in WT, mice. No apparent proteins were detected by anti-HA antibody, except for non-specific bands caused by the addition of antibodies (Ab, ~25 and ~50 kDa bands) for immunoprecipitation

Subcellular Localization of Nlgn1

To determine subcellular localization of endogenous Nlgn1 in vivo, we next performed immunohistochemical analysis of the *HA-Nlgn1* cerebellum using HA, PSD95 (postsynaptic density 95; an excitatory postsynaptic marker) and vGluT1 (a marker for parallel fiber terminals). We found that HA and PSD95 immunoreactivities were colocalized in the MLIs and the cerebellar glomeruli (Fig. 4a). In a higher magnification of an MLI (Fig. 4b, asterisk), which was co-immunostained for microtubule-associated protein 2 (MAP2), HA signals were mostly located on the soma and

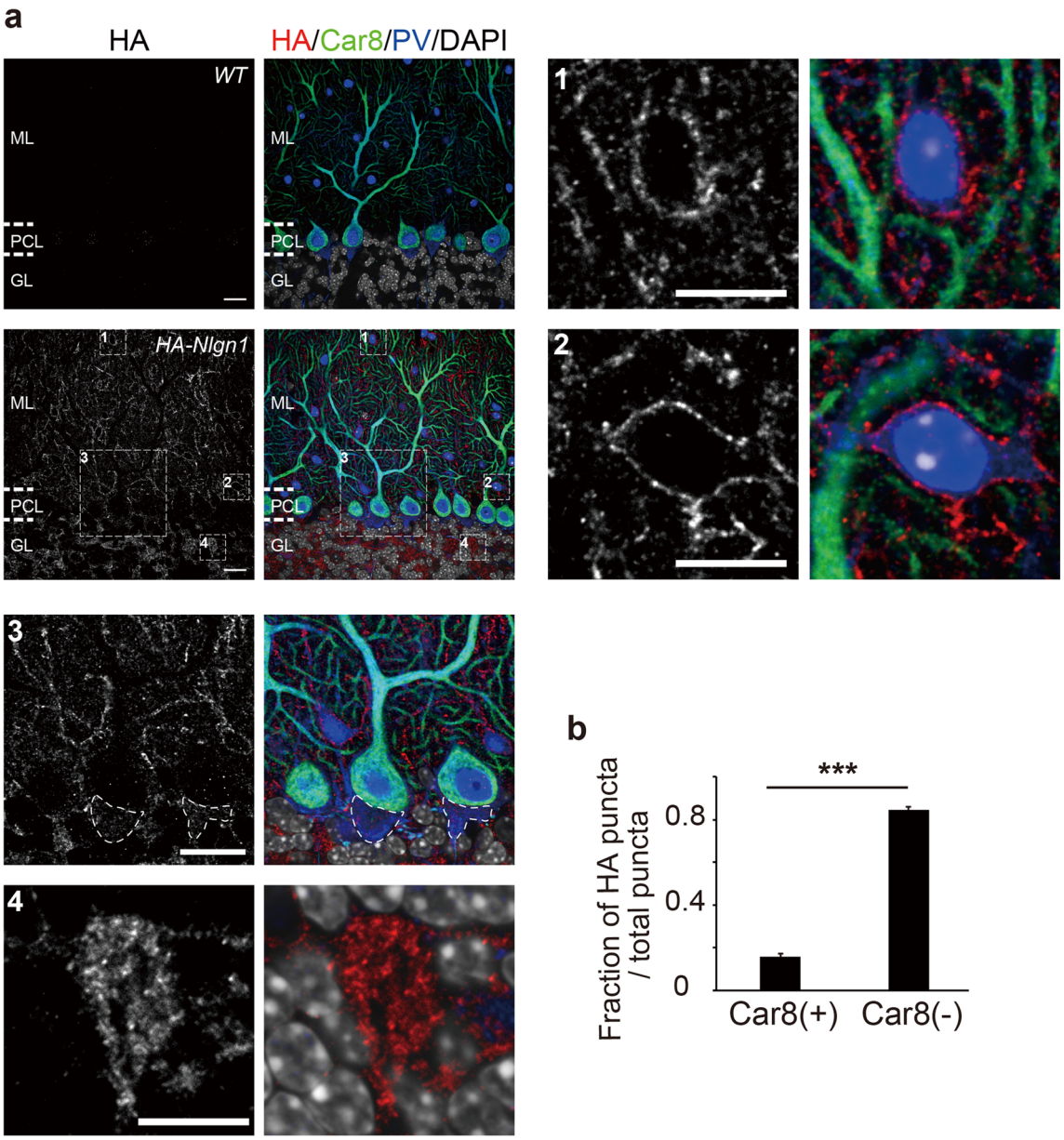

Fig. 3 Cellular localization of Nlgn1 in the cerebellar cortex. **a** Immunohistochemical analyses using antibodies against HA (red), Car8 (green, a marker for PCs), and PV (blue, a marker for PCs and MLIs), together with nuclear staining DAPI (white). HA signals were observed in *HA-Nlgn1* (lower panels), but not in wild-type (WT, upper panels) mice. ML molecular layer, PCL Purkinje cell layer, GL granular layer. Scale bar, 20 μm. Areas indicated by boxes are enlarged in the corresponding panels (1: stellate cell, 2: basket cell, 3, Purkinje cell, 4: glomerulus). Scale bar, 10 μm (boxes 1, 2, 4) and 20 μm (box 3). Note that relatively weak HA signals were observed in pinceau formation (dotted area in box 3), but not the cell body of Purkinje cells. **b** Quantification of the intensity of HA-immunopositive puncta in Car8–immunopositive [Car8(+)] and –immunonegative areas [Car8(−)]. Data represent means ± SEM. ***$p < 0.001$ based on the Mann-Whitney U test. $n = 9$ samples from three animals

dendrites (Fig. 4b, middle panels), and colocalized with PSD95 and vGluT1 signals (Fig. 4b, arrowheads in right panels, which show enlarged views of dotted boxes in the middle panel). Super-resolution microscopic analysis further revealed that, although HA, PSD95, and vGluT1 signals were colocalized, HA signals were located closer to PSD95 puncta (Fig. 4c). Similarly, we found that HA, PSD95, and vGluT1 signals were colocalized in the glomerulus of granule cells (Fig. 4d, arrowheads in the enlarged view). These results indicate that endogenous Nlgn1 is localized at the excitatory postsynaptic sites of PF-MLI and mossy fiber-granule cell synapses in the cerebellum.

Interestingly, we found HA-immunoreactive puncta in the basket-shaped pinceau (Fig. 3a, box 3, dotted line; Fig. 4e, dotted line), a specialized structure that modulates PC outputs

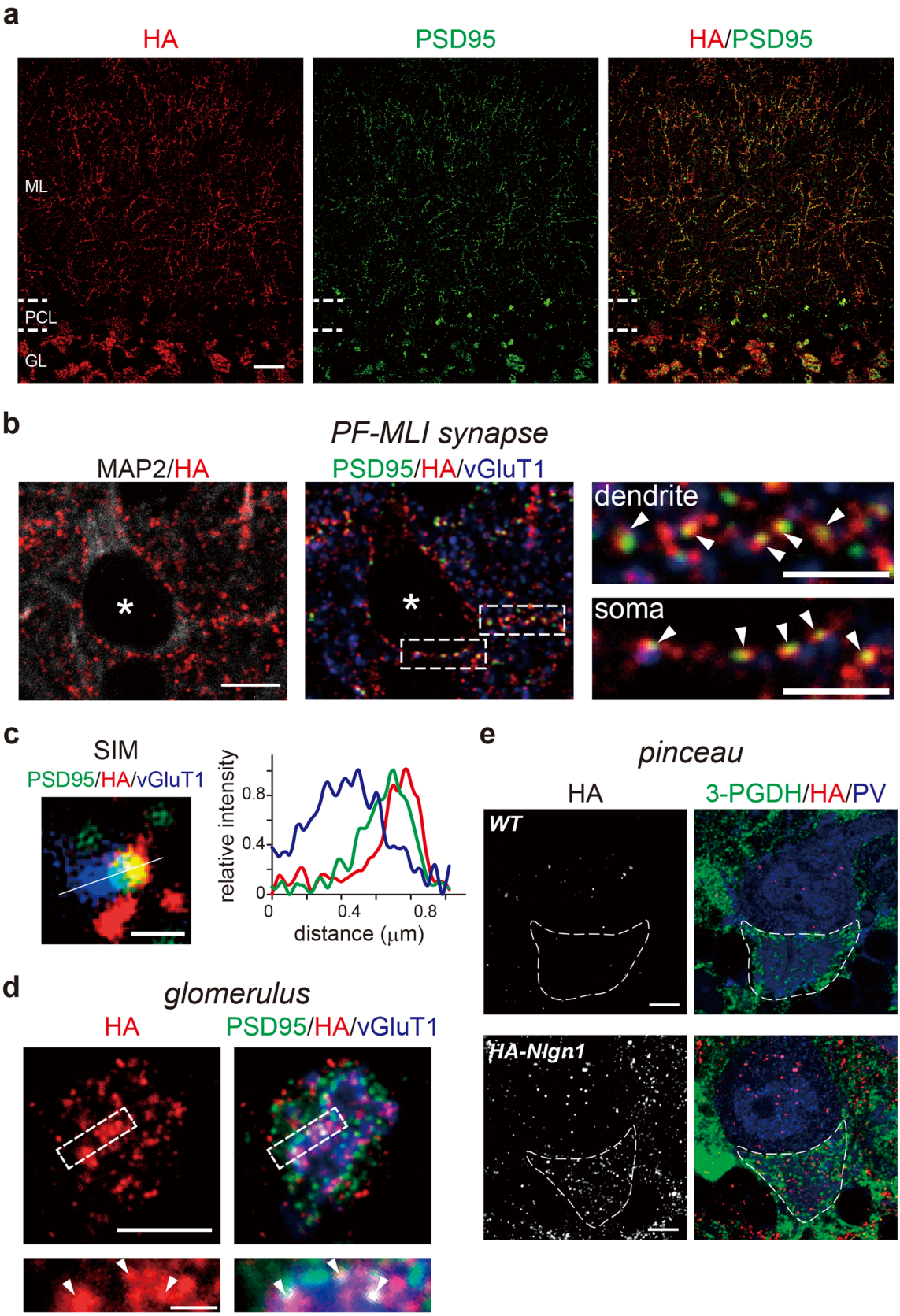
a
HA
PSD95
HA/PSD95
ML
PCL
GL
b
PF-MLI synapse
MAP2/HA
PSD95/HA/vGluT1
dendrite
soma
c
SIM
PSD95/HA/vGluT1
relative intensity
0.8
0.4
0
0
0.4
0.8
distance (μm)
d
glomerulus
HA
PSD95/HA/vGluT1
e
pinceau
HA
3-PGDH/HA/PV
WT
HA-Nlgn1

◀ **Fig. 4** Subcellular localization of Nlgn1. **a** Immunohistochemical analyses of *HA-Nlgn1* cerebellum using antibodies against HA (red) and PSD95 (green) showing that the HA-Nlgn1 and PSD95 signals grossly overlap in the cerebellar cortex. ML molecular layer, PCL Purkinje cell layer, GL granular layer. Scale bar, 20 μm. **b** Enlarged views of PF-MLI synapses immunostained for MAP2 (white), HA (red), PSD95 (green), and vGluT1 (blue). Boxes shown in the middle panel are further magnified in the panels to the right. HA-Nlgn1 was colocalized with PSD95 and vGluT1(arrowheads) in the dendrite (upper) and the soma (lower) of MLIs. Asterisks, nuclei of a MLI. Scale bar, left, 5 μm, right, magnified views, 2.5 μm. **c** Super-resolution microscopic analysis of subcellular localization of Nlgn1 at PF-MLI synapses. The right graph indicates HA (red), vGluT1 (blue), and PSD95 (green) immunoreactivities along the line indicated in the left panel. Scale bar, 0.5 μm. **d** Enlarged views of the glomerulus immunostained for HA (red), PSD95 (green), and vGluT1 (blue). Boxes shown in the top panels are magnified below. Arrowheads show colocalization of HA, PSD95, and vGluT1 immunoreactivities. Scale bar, top, 5 μm, magnified views, 1 μm. **e**. Enlarged views of the pinceau formation immunostained for HA (red), 3-PGDH (green), and PV (blue) in wild-type (WT, top panels) and *HA-Nlgn1* (bottom panels) mice. Scale bar, 5 μm

through electrical inhibition [23]. The pinceau is formed by finger-like processes of basket cell axons that do not make synapses with PC axon initial segments, which are separated by astrocytic elements [24, 25]. HA immunopositive puncta were located in the proximity of puncta immunopositive for PV, a marker for MLI axons in pinceau, and 3-phosphoglycerate dehydrogenase (3-PGDH), a marker for glial fibers (Fig. 4e). These results suggest that in addition to post-synaptic sites, some Nlgn1 proteins are localized at axons of MLIs and/or Bergmann glia.

AAV-Mediated Nlgn1 Knockdown Diminishes HA Signals in *HA-Nlgn1* Mice

To further validate that HA signals reflect the localization of HA-Nlgn1, we knocked down Nlgn1 by adeno-associated virus-mediated co-expression of GFP and shRNA against *Nlgn1* (AAV-sh-*Nlgn1*; Fig. 5a). Immunoblot analyses using HEK293 cells expressing HA-Nlgn1 and sh-*Nlgn1* showed that Nlgn1 was efficiently knocked down (Fig. 5b), as reported previously [19]. Immunohistochemical analyses revealed that AAV-mediated expression of GFP was limited to PV-positive MLIs and PCs, but not 3-PGDH-positive Bergmann glia (arrows) or DAPI-positive granule cells (Fig. 5c). We found that HA immunoreactivity mostly disappeared in the molecular layer of *HA-Nlgn1* mice injected with AAV-sh-*Nlgn1*, but not in those injected with control AAV (Fig. 5d). These results indicate that HA immunoreactivities in *HA-Nlgn1* mice reflect the endogenous localization of Nlgn1 proteins.

Importantly, HA-immunoreactivities in the pinceau were also significantly reduced by knockdown of Nlgn1 in *HA-Nlgn1* mice (Fig. 5e). Because AAV-sh-*Nlgn1* preferentially infected MLIs and PCs, but not Bergmann glia (Fig. 5c), Nlgn1 is most likely expressed in MLI axons in the pinceau. In contrast, knockdown of Nlgn1 did not cause significant changes in immunoreactivities of PSD95 and Kv1.2 (Fig. 5f), which are known to be enriched in MLI axons in the pinceau [24, 25], suggesting that Nlgn1 is dispensable for the recruitment of these molecules. Together, these results demonstrate the usefulness of *HA-Nlgn1* knock-in mice for the cellular and subcellular localization of endogenous Nlgn1.

Discussion

Despite the importance of synaptic organizers in defining functions of neuronal circuits, the cellular and subcellular localization of many synaptic organizers has remained largely elusive because of the paucity of specific antibodies for immunohistochemical studies. In the present study, taking advantage of a high-throughput electroporation-based gene editing technique with CRISPR/Cas9, we generated a knock-in mouse line in which an HA epitope was inserted into the *Nlgn1* gene. Using *HA-Nlgn1* mice, we have demonstrated the cellular and subcellular localization of endogenous Nlgn1 in cerebellar circuits (Fig. 5g), providing insights into cell- and synapse-specific roles of Nlgn1.

Cell-Type Specific Localization and Function of Nlgn1 in the Cerebellum

In the cerebellum, the mRNAs of Nlgn1, Nlgn2, and Nlgn3, but not Nlgn4, are highly expressed [5]. We found that endogenous Nlgn1 is highly enriched at PF-MLI synapses (Fig. 3a, boxes 1 and 2) and the glomerulus (Fig. 3a, box 4). Loss of Nlgn1 proteins in all, or a subset of, neurons results in reduced levels of extra-synaptic and synaptic NMDARs [26–30]. Indeed, in PV-driven *Nlgn1* knockout mice, in which Nlgn1 in PCs and MLIs are lost, PF-evoked excitatory postsynaptic currents (EPSCs) largely lacked NMDAR-dependent components [6]. While MLIs provide very fast feed-forward inhibition on PC activities by receiving PF inputs [31], activation of slow EPSCs mediated by NMDARs may play a role in temporal and spatial integration of PF inputs onto MLIs [6]. Thus, Nlgn1 expression in MLIs may be used to recruit NMDARs to endow slower EPSC components at PF-MLI synapses. In addition, long-term depression of synaptic transmission at PF-PC synapses, which is thought to mediate certain forms of motor learning in the cerebellum, is reported to depend on nitric oxide production, followed by PF-evoked NMDAR activation in MLIs [32]. Therefore, another role of enriched expression of Nlgn1 in MLIs may be to recruit NMDARs near synaptic sites to provide NO to spread plasticity across PF-PC synapses.

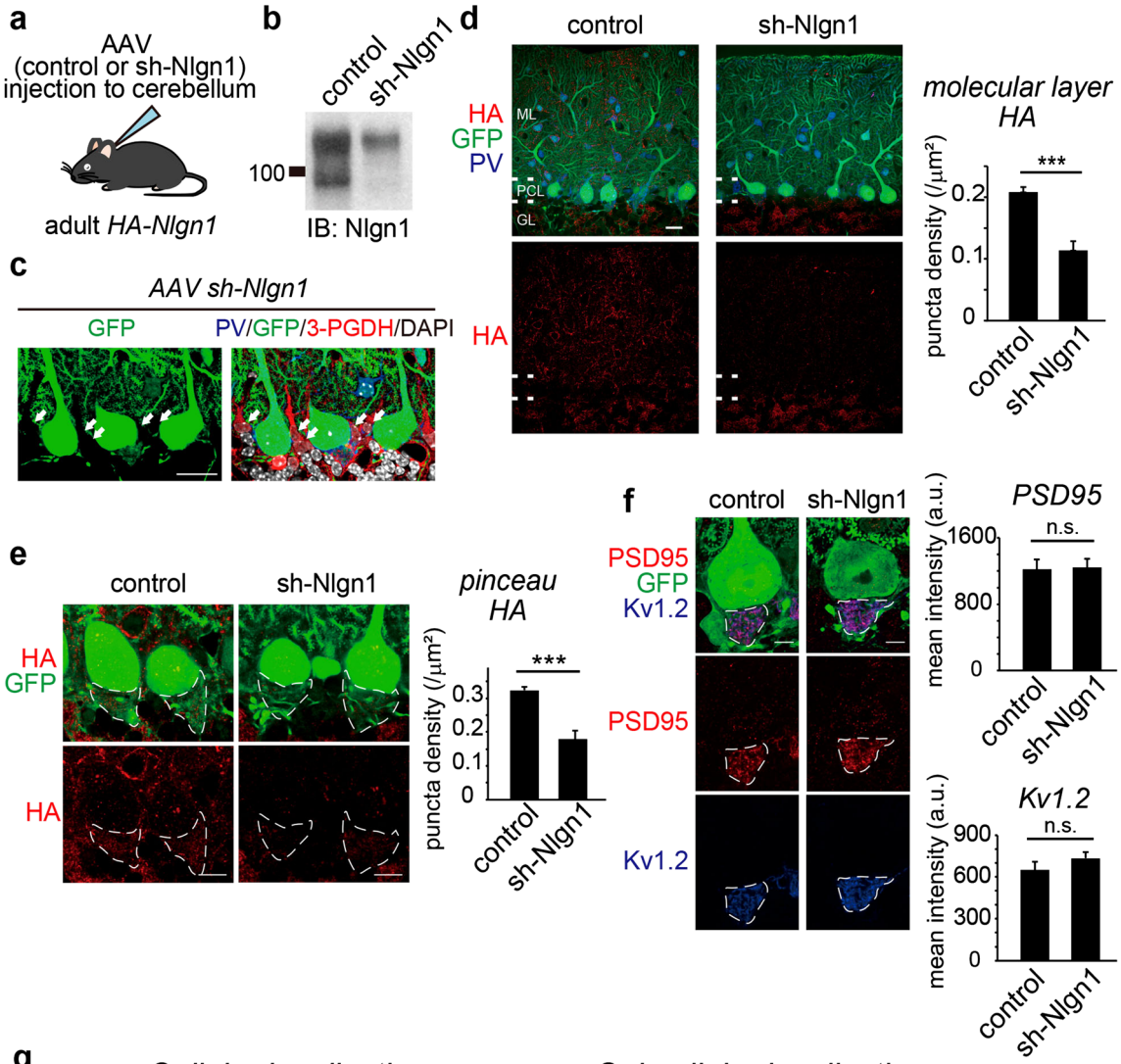
a
AAV
(control or sh-Nlgn1)
injection to cerebellum
adult HA-Nlgn1
b
control
sh-Nlgn1
100
IB: Nlgn1
c
AAV sh-Nlgn1
GFP
PV/GFP/3-PGDH/DAPI
d
control
sh-Nlgn1
HA
GFP
PV
ML
PCL
GL
HA
molecular layer
HA
puncta density (/μm²)
0.2
0.1
0
***
control
sh-Nlgn1
e
control
sh-Nlgn1
HA
GFP
HA
pinceau
HA
puncta density (/μm²)
0.3
0.2
0.1
0
***
control
sh-Nlgn1
f
control
sh-Nlgn1
PSD95
GFP
Kv1.2
PSD95
Kv1.2
PSD95
mean intensity (a.u.)
1600
800
0
n.s.
control
sh-Nlgn1
Kv1.2
mean intensity (a.u.)
900
600
300
0
n.s.
control
sh-Nlgn1
g
Cellular localization
PF
MLI
PC
pinceau
BC axon
GC
glomerulus
MF
• Nlgn1
Subcellular localization
PF-MLI
synapses
PF
MLI
pinceau
(BC axons)
glia
BC axon
glomeruli
(MF-GC synapses)
MF
GC dendrite
Nlgn1
Nrxns
PSD95
NMDAR
K⁺ channels

◀ **Fig. 5** Nlgn1 knockdown diminishes HA signals in *HA-Nlgn1* mice. a Schematics of AAV-mediated knockdown of Nlgn1. AAV encoding GFP plus shRNA against Nlgn1 (sh-Nlgn1) or no shRNA (control) were injected into the cerebellum of adult *HA-Nlgn1* mice. Immunohistochemical analyses were performed 14–21 days post-injection (dpi). **b** Knockdown efficiency of sh-Nlgn1. Lysates of HEK293 cells expressing HA-Nlgn1 plus sh-Nlgn1 or control were subjected to immunoblot analyses using anti-Nlgn1 antibody. **c** Immunohistochemical analyses of *HA-Nlgn1* cerebellum injected with AAV-sh-Nlgn1 using antibodies against GFP (green), 3-PGDH (red), and PV (blue), together with nuclear staining by DAPI. Note that AAV-mediated expression of GFP was limited to PV-positive MLIs and PCs, but not 3-PGDH-positive Bergmann glia (arrows) or DAPI-positive granule cells. Scale bar, 20 μm. **d** Nlgn1 knockdown largely reduces HA immunoreactivity in the molecular layer of the *HA-Nlgn1* cerebellum injected with AAV encoding sh-*Nlgn1* (right panels), but not control (left panels). Scale bar, 20 μm. The bottom graph shows quantification of HA signal density in these samples. ***$p < 0.001$ based on the Mann-Whitney *U* test. $n = 9$ regions from three animals. **e** Nlgn1 knockdown largely reduces HA immunoreactivity in the pinceau formation. The area designated by the dotted line indicates the pinceau. Scale bar, 5 μm. The bottom graph shows quantification of HA signal density in these samples. ***$p < 0.001$ based on the Mann-Whitney *U* test. $n = 12$ pinceau regions from 3 animals. Data represent means ± SEM. **f** Nlgn1 knockdown does not affect molecular markers of MLI axons in the pinceau formation. The left panels show the immunofluorescence of PSD95 (red) and Kv1.2 (blue). The dotted line indicates the pinceau. Scale bar, 5 μm. The right graphs show quantification of the immunoreactivity of PSD95 and Kv1.2 in the pinceau. n.s., not significant based on Mann-Whitney *U* test. $n = 15$ pinceau regions from three animals. Data represents means ± SEM. **g** Schematics of cellular and subcellular localization of endogenous Nlgn1 in the cerebellar cortex. Immunohistochemical studies using *HA-Nlgn1* mice indicate that endogenous Nlgn1 (left, red dots) is enriched at excitatory postsynaptic sites at PF-MLI synapses and the glomeruli, where mossy fibers (MF) make synapses with granule cell (GC) dendrites. In addition, Nlgn1 is localized at MLI axons in the pinceau formation

NMDARs are highly expressed in granule cells at mossy fiber-granule cell synapses in the glomerulus [33]. At these synapses, induction of long-term potentiation requires activation of postsynaptic NMDARs [34, 35]. Indeed, the genetic ablation of *Grin2a*, a subunit of NMDARs expressed in granule cells, did not affect basic synaptic transmission, but impaired LTP at these synapses, as well as visual adaptation of the vestibulo-ocular reflex, which is a form of cerebellum-dependent motor learning [36]. These findings indicate that highly enriched Nlgn1 expression in the glomerulus (Fig. 3a, box 4) likely plays a role in recruiting NMDARs to induce synaptic plasticity at mossy fiber-granule cell synapses.

Unlike most synapses in the central nervous system, PF-PC synapses lack functional NMDARs at postsynaptic sites [37]. Despite high expression levels of GluN1 mRNAs, immunohistochemical studies show very low GluN1 signals in PC dendrites in the molecular layer [33]. Thus, the weak expression of endogenous Nlgn1 immunopositive signals along PC dendrites (Fig. 3a, box 3) is consistent with the role of Nlgn1 in recruiting NMDARs. Indeed, the triple knockout of *Nlgn1–3* genes in PCs did not affect the number of PF-PC synapses [5], indicating that these synapses are mainly regulated by the δ2 glutamate receptor (GluD2) and Cbln1 as synaptic organizers [38]. In contrast, climbing fiber (CF)-evoked small NMDAR currents have been recently reported in mature PCs [39]. In addition, PC-specific *Nlgn1* knockout mice showed small (~ 5%) reduction in CF-evoked EPSCs [5], reflecting that Cbln1-GluD2 are not expressed at CF-PC synapses [38]. Thus, postsynaptic NMDARs may be recruited by a small amount of Nlgn1 at these synapses.

Subcellular Localization of Nlgn1 in the Cerebellum

Although endogenous Nlgn1 was originally shown to be selectively localized at excitatory postsynaptic sites [40], antibodies (4C12 and 5G10) used in this study gave rise to non-specific signals in triple *Nlgn1–3* knockout mice [5]. In addition, overexpression of epitope-tagged Nlgn1 can induce both excitatory and inhibitory synapses in vitro [19, 41]. In the present study, we found that HA-Nlgn1 was highly colocalized with excitatory pre- (vGluT1) and postsynaptic (PSD95) markers at PF-MLI synapses (Fig. 4b, c) and the glomerulus (Fig. 4d) in the cerebellum. Although further quantitative immunoelectron microscopic studies are necessary, these results indicate that endogenous Nlgn1 is predominantly localized at the excitatory synapses.

Interestingly, we also found that Nlgn1 is localized in the pinceau (Fig. 4e). Because HA immunoreactivity in the pinceau was largely reduced by knocking down Nlgn1 in MLIs (Fig. 5e), basket cell axons likely express Nlgn1. Unlike axo-axonic terminals in the cerebral cortex, basket cell axon terminals highly express Shaker-type potassium channels and their scaffolding protein PSD95 [24, 25]. Together with the lack of sodium channels at axon terminals, these features enable the pinceau formation to generate a strong inhibitory electrical field without action potentials [42]. Although Nlgn1 binds to PSD95 [43] and overexpression of Nlgn1 recruits PSD95 in neurons [19, 41], knockdown of Nlgn1 did not cause significant changes in the localization of PSD95 and Kv1.2 in the pinceau (Fig. 5f), suggesting that Nlgn1 is dispensable for recruitment of these molecules. Alternatively, other Nlgn family members may compensate for the loss of Nlgn1 [5]. Interestingly, finger-like processes of basket cell axons are separated from PC axons by astrocytic septate-like junctions in the pinceau [24, 25]. Because astrocyte morphology has recently been shown to be regulated by Nrxn-Nlgn interaction between neurons and glia [44], Nlgn1 may also be involved in the formation of elaborate astrocytic processes in the pinceau. Future studies are warranted to clarify how Nlgn1 is recruited to and functions in the pinceau formation.

Subpopulation of Nlgn1 Indistinguishable in *HA-Nlgn1* Knock-in Mice

The extracellular domain of Nlgn1 is shed by proteolytic cleavage at the stalk region near the transmembrane domain [45, 46]. If the cleaved fragment remains in the same region of the tissue, our immunohistochemical analyses would be unable to distinguish the cleaved fragment from the full-length Nlgn1 because the epitope-tag was attached to the N-terminus of Nlgn1. However, immunoblot analyses with anti-HA antibody after immunoprecipitation of HA-tagged proteins failed to detect cleaved fragments of Nlgn1 (< 100 kDa) (Fig. 2e). These results indicate that, unlike during development, cleavage of Nlgn1 may not occur frequently in the adult brain [46]. Thus, the HA immunoreactivities that we observed in the *HA-Nlgn1* knock-in cerebellum most likely represent full-length Nlgn1, but not its cleaved fragments.

Nlgn1 has two alternative splicing sites, A and B [47]. As mentioned previously, these splice isoforms are indistinguishable in *HA-Nlgn1* knock-in mice. Using electroporation-based gene editing with CRISPR/Cas9, it would be possible to generate knock-in mice in which epitope tags are inserted at each splice site. However, it remains challenging to introduce epitope tags into short splice sites present in many synaptic organizers, such as Nrxn [48, 49] and receptor protein tyrosine phosphatase δ [50], because certain splice sites are in the proximity of protein interaction domains. For example, modification near splice site B of Nlgn1 inevitably affects its binding to α-Nrxn [51, 52]. Therefore, further development of new technologies to label endogenous synaptic organizers without affecting their functions is highly warranted.

Funding This work was supported by JSPS KAKENHI (JP16H06461) and MEXT KAKENHI (JP15H05772) and JST CREST (JPMJCR13L6).

Compliance with Ethical Standards

Conflict of Interest The authors declare that they have no competing interests.

References

1. Satterthwaite TD, Baker JT. How can studies of resting-state functional connectivity help us understand psychosis as a disorder of brain development? Curr Opin Neurobiol. 2015;30:85–91.
2. Ameis SH, Catani M. Altered white matter connectivity as a neural substrate for social impairment in autism spectrum disorder. Cortex. 2015;62:158–81.
3. Sudhof TC. Neuroligins and neurexins link synaptic function to cognitive disease. Nature. 2008;455:903–11.
4. Forrest MP, Parnell E, Penzes P. Dendritic structural plasticity and neuropsychiatric disease. Nat Rev Neurosci. 2018;19:215–34.
5. Zhang B, Chen LY, Liu X, Maxeiner S, Lee SJ, Gokce O, et al. Neuroligins sculpt cerebellar Purkinje-cell circuits by differential control of distinct classes of synapses. Neuron. 2015;87:781–96.
6. Zhang B, Sudhof TC. Neuroligins are selectively essential for NMDAR signaling in cerebellar stellate interneurons. J Neurosci. 2016;36:9070–83.
7. Miura E, Matsuda K, Morgan JI, Yuzaki M, Watanabe M. Cbln1 accumulates and colocalizes with Cbln3 and GluRdelta2 at parallel fiber-Purkinje cell synapses in the mouse cerebellum. Eur J Neurosci. 2009;29:693–706.
8. Yang J, Siao CJ, Nagappan G, Marinic T, Jing D, McGrath K, et al. Neuronal release of proBDNF. Nat Neurosci. 2009;12:113–5.
9. Yang H, Wang H, Shivalila CS, Cheng AW, Shi L, Jaenisch R. One-step generation of mice carrying reporter and conditional alleles by CRISPR/Cas-mediated genome engineering. Cell. 2013;154:1370–9.
10. Mikuni T, Nishiyama J, Sun Y, Kamasawa N, Yasuda R. High-throughput, high-resolution mapping of protein localization in mammalian brain by in vivo genome editing. Cell. 2016;165:1803–17.
11. Hashimoto M, Takemoto T. Electroporation enables the efficient mRNA delivery into the mouse zygotes and facilitates CRISPR/Cas9-based genome editing. Sci Rep. 2015;5:11315.
12. Chen S, Lee B, Lee AY, Modzelewski AJ, He L. Highly efficient mouse genome editing by CRISPR ribonucleoprotein electroporation of zygotes. J Biol Chem. 2016;291:14457–67.
13. Kawai S, Takagi Y, Kaneko S, Kurosawa T. Effect of three types of mixed anesthetic agents alternate to ketamine in mice. Exp Anim. 2011;60:481–7.
14. Dehairs J, Talebi A, Cherifi Y, Swinnen JV. CRISP-ID: decoding CRISPR mediated indels by Sanger sequencing. Sci Rep. 2016;6:28973.
15. Matsuda K, Yuzaki M. Cbln family proteins promote synapse formation by regulating distinct neurexin signaling pathways in various brain regions. Eur J Neurosci. 2011;33:1447–61.
16. Matsuda S, Kakegawa W, Budisantoso T, Nomura T, Kohda K, Yuzaki M. Stargazin regulates AMPA receptor trafficking through adaptor protein complexes during long-term depression. Nat Commun. 2013;4:2759.
17. Matsuda K, Budisantoso T, Mitakidis N, Sugaya Y, Miura E, Kakegawa W, et al. Transsynaptic modulation of Kainate receptor functions by C1q-like proteins. Neuron. 2016;90:752–67.
18. Schindelin J, Arganda-Carreras I, Frise E, Kaynig V, Longair M, Pietzsch T, et al. Fiji: an open-source platform for biological-image analysis. Nat Methods. 2012;9:676–82.
19. Chih B, Engelman H, Scheiffele P. Control of excitatory and inhibitory synapse formation by neuroligins. Science. 2005;307:1324–8.
20. Kakegawa W, Mitakidis N, Miura E, Abe M, Matsuda K, Takeo YH, et al. Anterograde C1ql1 signaling is required in order to determine and maintain a single-winner climbing fiber in the mouse cerebellum. Neuron. 2015;85:316–29.
21. Budreck EC, Kwon OB, Jung JH, Baudouin S, Thommen A, Kim HS, et al. Neuroligin-1 controls synaptic abundance of NMDA-type glutamate receptors through extracellular coupling. Proc Natl Acad Sci U S A. 2013;110:725–30.
22. Scheiffele P, Fan J, Choih J, Fetter R, Serafini T. Neuroligin expressed in nonneuronal cells triggers presynaptic development in contacting axons. Cell. 2000;101:657–69.
23. Blot A, Barbour B. Ultra-rapid axon-axon ephaptic inhibition of cerebellar Purkinje cells by the pinceau. Nat Neurosci. 2014;17:289–95.
24. Laube G, Roper J, Pitt JC, Sewing S, Kistner U, Garner CC, et al. Ultrastructural localization of shaker-related potassium channel subunits and synapse-associated protein 90 to septate-like junctions in rat cerebellar Pinceaux. Brain Res Mol Brain Res. 1996;42:51–61.
25. Iwakura A, Uchigashima M, Miyazaki T, Yamasaki M, Watanabe M. Lack of molecular-anatomical evidence for GABAergic

influence on axon initial segment of cerebellar Purkinje cells by the pinceau formation. J Neurosci. 2012;32:9438–48.
26. Chubykin AA, Atasoy D, Etherton MR, Brose N, Kavalali ET, Gibson JR, et al. Activity-dependent validation of excitatory versus inhibitory synapses by neuroligin-1 versus neuroligin-2. Neuron. 2007;54:919–31.
27. Kim J, Jung SY, Lee YK, Park S, Choi JS, Lee CJ, et al. Neuroligin-1 is required for normal expression of LTP and associative fear memory in the amygdala of adult animals. Proc Natl Acad Sci U S A. 2008;105:9087–92.
28. Blundell J, Blaiss CA, Etherton MR, Espinosa F, Tabuchi K, Walz C, et al. Neuroligin-1 deletion results in impaired spatial memory and increased repetitive behavior. J Neurosci. 2010;30:2115–29.
29. Soler-Llavina GJ, Fuccillo MV, Ko J, Sudhof TC, Malenka RC. The neurexin ligands, neuroligins and leucine-rich repeat transmembrane proteins, perform convergent and divergent synaptic functions in vivo. Proc Natl Acad Sci U S A. 2011;108:16502–9.
30. Kwon HB, Kozorovitskiy Y, Oh WJ, Peixoto RT, Akhtar N, Saulnier JL, et al. Neuroligin-1-dependent competition regulates cortical synaptogenesis and synapse number. Nat Neurosci. 2012;15:1667–74.
31. Mittmann W, Koch U, Hausser M. Feed-forward inhibition shapes the spike output of cerebellar Purkinje cells. J Physiol. 2005;563:369–78.
32. Shin JH, Linden DJ. An NMDA receptor/nitric oxide cascade is involved in cerebellar LTD but is not localized to the parallel fiber terminal. J Neurophysiol. 2005;94:4281–9.
33. Yamada K, Fukaya M, Shimizu H, Sakimura K, Watanabe M. NMDA receptor subunits GluRepsilon1, GluRepsilon3 and GluRzeta1 are enriched at the mossy fibre-granule cell synapse in the adult mouse cerebellum. Eur J Neurosci. 2001;13:2025–36.
34. D'Angelo E, Rossi P, Armano S, Taglietti V. Evidence for NMDA and mGlu receptor-dependent long-term potentiation of mossy fiber-granule cell transmission in rat cerebellum. J Neurophysiol. 1999;81:277–87.
35. Sola E, Prestori F, Rossi P, Taglietti V, D'Angelo E. Increased neurotransmitter release during long-term potentiation at mossy fibre-granule cell synapses in rat cerebellum. J Physiol. 2004;557:843–61.
36. Andreescu CE, Prestori F, Brandalise F, D'Errico A, De Jeu MT, Rossi P, et al. NR2A subunit of the N-methyl D-aspartate receptors are required for potentiation at the mossy fiber to granule cell synapse and vestibulo-cerebellar motor learning. Neuroscience. 2011;176:274–83.
37. Perkel DJ, Hestrin S, Sah P, Nicoll RA. Excitatory synaptic currents in Purkinje cells. Proc Biol Sci. 1990;241:116–21.
38. Matsuda K, Miura E, Miyazaki T, Kakegawa W, Emi K, Narumi S, et al. Cbln1 is a ligand for an orphan glutamate receptor delta2, a bidirectional synapse organizer. Science. 2010;328:363–8.
39. Piochon C, Levenes C, Ohtsuki G, Hansel C. Purkinje cell NMDA receptors assume a key role in synaptic gain control in the mature cerebellum. J Neurosci. 2010;30:15330–5.
40. Song JY, Ichtchenko K, Sudhof TC, Brose N. Neuroligin 1 is a postsynaptic cell-adhesion molecule of excitatory synapses. Proc Natl Acad Sci U S A. 1999;96:1100–5.
41. Prange O, Wong TP, Gerrow K, Wang YT, El-Husseini A. A balance between excitatory and inhibitory synapses is controlled by PSD-95 and neuroligin. Proc Natl Acad Sci U S A. 2004;101:13915–20.
42. Korn H, Axelrad H. Electrical inhibition of Purkinje cells in the cerebellum of the rat. Proc Natl Acad Sci U S A. 1980;77:6244–7.
43. Irie M, Hata Y, Takeuchi M, Ichtchenko K, Toyoda A, Hirao K, et al. Binding of neuroligins to PSD-95. Science. 1997;277:1511–5.
44. Stogsdill JA, Ramirez J, Liu D, Kim YH, Baldwin KT, Enustun E, et al. Astrocytic neuroligins control astrocyte morphogenesis and synaptogenesis. Nature. 2017;551:192–7.
45. Suzuki K, Hayashi Y, Nakahara S, Kumazaki H, Prox J, Horiuchi K, et al. Activity-dependent proteolytic cleavage of neuroligin-1. Neuron. 2012;76:410–22.
46. Peixoto RT, Kunz PA, Kwon H, Mabb AM, Sabatini BL, Philpot BD, et al. Transsynaptic signaling by activity-dependent cleavage of neuroligin-1. Neuron. 2012;76:396–409.
47. Ichtchenko K, Hata Y, Nguyen T, Ullrich B, Missler M, Moomaw C, et al. Neuroligin 1: a splice site-specific ligand for beta-neurexins. Cell. 1995;81:435–43.
48. Treutlein B, Gokce O, Quake SR, Sudhof TC. Cartography of neurexin alternative splicing mapped by single-molecule long-read mRNA sequencing. Proc Natl Acad Sci U S A. 2014;111:E1291–9.
49. Schreiner D, Nguyen TM, Russo G, Heber S, Patrignani A, Ahrne E, et al. Targeted combinatorial alternative splicing generates brain region-specific repertoires of neurexins. Neuron. 2014;84:386–98.
50. Yamagata A, Yoshida T, Sato Y, Goto-Ito S, Uemura T, Maeda A, et al. Mechanisms of splicing-dependent trans-synaptic adhesion by PTPdelta-IL1RAPL1/IL-1RAcP for synaptic differentiation. Nat Commun. 2015;6:6926.
51. Boucard AA, Chubykin AA, Comoletti D, Taylor P, Sudhof TC. A splice code for trans-synaptic cell adhesion mediated by binding of neuroligin 1 to alpha- and beta-neurexins. Neuron. 2005;48:229–36.
52. Chih B, Gollan L, Scheiffele P. Alternative splicing controls selective trans-synaptic interactions of the neuroligin-neurexin complex. Neuron. 2006;51:171–8.